International Journal of Pharmaceutics 597 (2021) 120280

Contents lists available at ScienceDirect

International Journal of Pharmaceutics

journal homepage: www.elsevier.com/locate/ijpharm

PLGA encapsulated γ-cyclodextrin-meropenem inclusion complex formulation for oral delivery

Aun Raza [a,b], Jared A. Miles [a], Fekade Bruck Sime [a,b], Benjamin P. Ross [a], Jason A. Roberts [a,b,c,d], Amirali Popat [a,e,*], Tushar Kumeria [a,f,*], James R. Falconer [a,*]

[a] School of Pharmacy, The University of Queensland, Woolloongabba 4102, Australia
[b] Centre for Translational Anti-infective Pharmacodynamics, School of Pharmacy, The University of Queensland, Woolloongabba 4102, QLD, Australia
[c] Department of Intensive Care Medicine, Royal Brisbane and Women's Hospital, Brisbane 4029, QLD, Australia
[d] Department of Pharmacy, Royal Brisbane and Women's Hospital, Brisbane 4029, QLD, Australia
[e] Mucosal Diseases Group, Mater Research Institute – The University of Queensland, Translational Research Institute, 37 Kent St, Woolloongabba, QLD 4102, Australia
[f] School of Materials Science and Engineering, The University of New South Wales, Sydney NSW-2052, Australia

ARTICLE INFO

Keywords:
Cyclodextrins
Liquid CO_2
Meropenem
Oral antibiotics
Oral drug delivery
PLGA nanoparticles

ABSTRACT

Meropenem (MER) is one of the last resort antibiotics used to treat resistant bacterial infections. However, the clinical effectiveness of MER is hindered due to chemical instability in aqueous solution and gastric pH, and short plasma half-life. Herein, a novel multi-material delivery system based on γ-cyclodextrin (γ-CD) and poly lactic-co-glycolic acid (PLGA) is demonstrated to overcome these challenges. MER showed a saturated solubility of 14 mg/100 mL in liquid CO_2 and later it was loaded into γ-CD to form the inclusion complex using the liquid CO_2 method. The γ-CD and MER inclusion complex (MER-γ-CD) was encapsulated into PLGA by the well-established double emulsion solvent evaporation method. The formation of the inclusion complex was confirmed using FTIR, XRD, DSC, SEM, and ^{1}H NMR and docking study. Further, MER-γ-CD loaded PLGA nanoparticles (MER-γ-CD NPs) were characterized by SEM, DLS, and FTIR. The drug loading and entrapment efficiency for MER-γ-CD were 21.9 and 92. 2% *w/w*, respectively. However, drug loading and entrapment efficiency of MER-γ-CD NPs was significantly lower at up to 3.6 and 42.1% *w/w*, respectively. In vitro release study showed that 23.6 and 27.4% of active (non-degraded drug) and total drug (both degraded and non-degraded drug) were released from MER-γ-CD NPs in 8 h, respectively. The apparent permeability coefficient (Papp) (A to B) for MER, MER-γ-CD, and MER-γ-CD NPs were 2.63 × 10^{-6} cm/s, 2.81 × 10^{-6} cm/s, and 2.92 × 10^{-6} cm/s, respectively. For secretory transport, the Papp (B to A) were 1.47 × 10^{-6} cm/s, 1.53 × 10^{-6} cm/s, and 1.58 × 10^{-6} cm/s for MER, MER-γ-CD and MER-γ-CD NPs, respectively. Finally, the MER-γ-CD inclusion complex and MER-γ-CD NPs retained MER's antibacterial activities against *Staphylococcus aureus* and *Pseudomonas aeruginosa*. Overall, this work demonstrates the significance of MER-γ-CD NPs to protect MER from gastric pH with controlled drug release, while retaining MER's antibacterial activity.

1. Introduction

Meropenem (MER) belongs to the carbapenem group of the β-lactam class of antibiotics and is only parenterally administered for treatment of an ultrabroad spectrum of Gram-negative and Gram-positive bacteria (Baldwin et al., 2008; Craig, 1997). MER inhibits bacterial wall synthesis, similar to other β-lactams, however, its resistance against degradation by beta-lactamases or cephalosporinases is uncommon in β-lactams (Raza et al., 2020). Moreover, carbapenems are now powerful antibiotic drugs of last resort to treat many multidrug-resistant bacterial infections (Craig, 1997; Nicolau, 2008). Like other carbapenems, MER also undergoes hydrolysis resulting in β-lactam ring-opening and consequent loss of its bactericidal properties (Fawaz et al., 2019). Thus, MER is only marketed as a powder for the preparation of the parenteral solution. A study by Fawaz et al. illustrated that MER could be continuously infused to patients for at least 7 h or 5 h at 22 °C or 33 °C, respectively (Fawaz et al., 2019). Also, solid-state stability studies showed that carbapenems such as MER and tebipenem are also unstable at 40 °C after 5 h and undergo thermolysis, which could also produce toxic degradation products (Cielecka-Piontek et al., 2013; Talaczyńska

* Corresponding authors at: 20 Cornwall St, School of Pharmacy, The University of Queensland, Woolloongabba, QLD 4102, Australia.
E-mail addresses: a.popat@uq.edu.au (A. Popat), t.kumeria@unsw.edu.au (T. Kumeria), j.falconer@uq.edu.au (J.R. Falconer).

https://doi.org/10.1016/j.ijpharm.2021.120280
Received 29 November 2020; Received in revised form 7 January 2021; Accepted 8 January 2021
Available online 1 February 2021

et al., 2016). This chemical instability coupled with fast renal elimination (i.e. short half-life of around 1 h) necessitates short-term intravenous bolus injections (typically 5 min) after dosage preparation (<1.0 h) (Craig, 1997; Mendez et al., 2006). These challenges demand frequent administration of MER with other healthcare facilities such as temperature-controlled environment to minimize MER degradation, and pharmacy and nursing staff for frequent preparation and administration of MER, respectively. Therefore, after IV MER administration, once the health of the patient improves, switching to oral treatment has multiple advantages, including short inpatient admission with lower nursing cost and increased patient compliance. Therefore, developing oral formulations of such antimicrobials including MER is warranted for IV to oral antimicrobial switch therapies for outpatients. Unfortunately, MER suffers from poor oral bioavailability due to its hydrophilicity – inhibiting the passive diffusion across the GI epithelium, instability in the gastric environment, and GI expulsion through enterocyte efflux glycoproteins (MDR1, ABCB1) (Saito et al., 2012).

To overcome the above-mentioned limitations of MER, there have been efforts to stabilize the MER by incorporating it into cyclodextrins (CDs), such as β-CD and hydroxypropyl- β-CD(HP- β-CD) (Paczkowska et al., 2016; Wong et al., 2014). However, all of these were intended for parenteral dosing. Naturally occurring CDs comprise of oligosaccharides consisting of 6, 7, or 8 rings of D-glucopyranose to form α-CD, β-CD, and γ-CD, respectively. Guest–host complexes involving CDs are currently applied in therapeutic systems for parenteral drug delivery (e.g. paclitaxel) and for oral drug administration (e.g. salbutamol, diltiazem) (Rasheed, 2008; Raza et al., 2017b). Among these, γ-CD is considered most suitable for oral drug delivery due to its higher water solubility and susceptibility to hydrolysis by α-amylase, reducing the chances of gastrointestinal disturbance. Comparatively, α-CD (Carrier et al., 2007; Rasheed, 2008) cause sub chronic oral toxicity including diarrhoea, and less food consumption (Lina and Bär, 2004), while the Joint Food and Agriculture Organization of the United Nations and World Health Organization (FAO/WHO) Expert Committee on Food Additives (JECFA) has placed restrictions on the daily intake of β-CD as a food additive (Joint et al., 2005).

Different conventional techniques such as kneading and freeze-drying have been extensively employed to produce pharmaceutical formulation containing CDs. Nevertheless, various drawbacks of these methods including long processing time, low loading efficiency, and presence of residual organic solvents in the final formulation demand for an alternative method (Lee et al., 2008). It is reported that carbon dioxide in its supercritical or liquid state can be used as an alternative solvent because of its ability to evacuate after depressurization and produce a solvent-free formulation (Kankala et al., 2017; Raza Aun and Popat, 2020). Also, $scCO_2$/liquid CO_2 works at low temperatures therefore, this solvent is suitable for temperature-sensitive compounds (Pasquali and Bettini, 2008).

Studies showed that poly (lactic-*co*-glycolic acid) (PLGA) nanoparticles (NPs) have been widely used as a nano-carrier in drug delivery because of its clinically proven biodegradability and biocompatibility (Avgoustakis, 2004; Blanco and Alonso, 1997; Ghaferi et al., 2020a; Raza et al., 2017a; Sarti et al., 2011). In addition, encapsulation of antimicrobial agents into biodegradable and biocompatible nanoparticles potentially allows controlled drug release over time, thus prolonging the drug circulation half-life and maintaining the therapeutic concentration of the drug at the site of infection (Lim et al., 2016). Furthermore, nano-encapsulation reduces the dose and frequency of administration, minimize side effects, and enhance the pharmacokinetic profile of the drug, in addition to overcoming potential solubility and stability issues. Antimicrobial-loaded nanoparticles have also been shown to contribute to overcoming antimicrobial resistance via increasing intracellular uptake, reducing the efflux of drugs (Ghaferi et al., 2020b; Pelgrift and Friedman, 2013; Raza Aun and Popat, 2020; Zhang et al., 2010).

In this work, as none of the previously presented studies has explored the combination of γ-CD and PLGA for oral delivery of MER, we formulated MER with γ-CD using the liquid CO_2 method and encapsulated the MER-γ-CD inclusion complex into PLGA NPs using the double emulsion method. The rationale behind using PLGA NPs was to protect MER from gastric pH with controlled drug release. For this, we systematically investigated the solubility of MER in liquid CO_2 before preparing the MER-γ-CD inclusion complex. The present work aimed to prepare and characterize PLGA nanoparticles loaded with the MER-γ-CD complex to achieve changes in drug release, Caco-2 permeability, and antibacterial activity.

2. Materials and methods

2.1. Materials

Meropenem trihydrate of analytical standard ≥98% was purchased from Fujifilm Wako Pure Chemical Corporation, China. The γ-cyclodextrin (CD) was from TCI (Tokyo Chemical Industry, Japan). Poly(D,L-lactide-co-glycolide) (PLGA, acid terminated, lactide:glycolide 50:50, M_w 24,000–38,000) was purchased from Sigma-Aldrich (Australia). Sodium hydroxide (NaOH), phosphoric acid (H_3PO_4), hydrochloric acid (HCl, 32% w/w), acetonitrile (HPLC grade), dichloromethane (DCM), and dipotassium hydrogen orthophosphate anhydrous was purchased from Chem-Supply (Gillman, SA, Australia). Polyvinyl alcohol purchased from Sigma-Aldrich (Australia) was 87–89% hydrolyzed with a molecular weight of 13,000–23,000. MTT (3-(4,5-dimethyl-2-thiazolyl)-2,5-diphenyl-2H-tetrazolium bromide) reagent and cyanine5 NHS ester (Cy-5) were purchased from Tocris Bioscience, Australia. Dulbecco's modified eagle medium (DMEM) with phenol red (D6556 and D5796) and without phenol red (D8537), Dulbecco's phosphate-buffered saline (PBS), fetal bovine serum (FBS), Triton X-100, paraformaldehyde, MEM non-essential amino acid solution (100X), phalloidin-FITC (fluorescein isothiocyanate) and DAPI (4′,6-diamidino-2-phenylindole) were purchased from Sigma-Aldrich, Australia. Pen-Strep (Penicillin 10,000 U/mL and Streptomycin 10,000 μg/mL), Hank's balanced salt solution (HBSS), 0.25% Trypsin-EDTA (1X), L-glutamine (100X) and sodium pyruvate (100 mM) from Gibco; Thermo Fisher Scientific, Australia. A liquid CO_2 cylinder was purchased from BOC Australia. Ultrapure deionized water with a resistivity of 18.2 MΩ was (Millipore Milli-Q) used for the preparation of all the aqueous solutions.

2.2. Determination of MER solubility in liquid CO_2

A gravimetric method by Sherman, et al. (Sherman et al., 2000) was used as the basis and adapted to determine the solubility of MER in liquid CO_2. Briefly, stainless steel (SS) sample holder having an internal diameter of 19 mm was used to weigh 50 mg of MER (as a starting point) and covered with SS mesh (210 μm pore size) and clamp (**Figure S1, Supporting information**). The sample holder was placed into a 60 mL marine-grade 316-SS vessel (Nottingham, UK) and a syringe pump (Teledyne Isco Series 260 D with a controller, Lincoln, USA) was used to pump liquid CO_2 into the SS vessel at a pressure of 60 bar and the vessel was placed in an ice bath to maintain the temperature at 6–8 °C. Stirring set to 200 RPM, with a small paddle (Parr Systems, USA) was used to agitate the bulk volume (at the top of the 60 mL solvent vessel, to not be directly above the sample holder using an overhead motor. A set of MER solubility experiments were carried out on separate samples for each time point (up to 18 h or to where 3 data points were similar i.e. flattening of the curve. At the end of each experiment, the vessel was allowed to depressurize completely then opened to remove the sample holder and weighed. The difference between the weight of the sample holder containing MER before and after the experiment was used as an indirect way to determine the MER solubility.

To investigate the effect of cosolvent (water) on MER solubility, the solubility of MER (30 mg) was also determined in liquid CO_2 (4 h).

2.3. Stoichiometry determination: Job's method

Job's method (Job, 1928) (also called continuous variation method) was employed to investigate the stoichiometry of the host-guest inclusion complexes using Cary 60 UV–Vis spectrophotometer (Agilent Technologies, USA) in the range of 200–400 nm. A series of solutions (0–30 μM) for MER and γ -CD were generated with the different mole fraction of the MER in the range 0–1 and their absorbance values were measured at 298 nm. Job's plot was established by plotting ΔA × R against R, representing ΔA as a difference in absorbance of the MER without and with γ-CD and R = [MER]/([MER] + [γ -CD]). The maximum deviation value of R provides the stoichiometry of the inclusion complex.

2.4. Effects of γ-CD on the UV–vis absorption spectra of MER

The UV–vis spectrophotometric studies of the interactions of host with guest molecule can be used to determine the effect of host on guest molecule through the spectral changes related to the formation of the inclusion complexes. In this study, the absorption spectra of MER (0.1 mM) was observed with increasing the concentration of γ-CD (0.2–0.5 mM) to find out the effects of γ-CD on MER.

2.5. Preparation of MER-γ-CD inclusion complex

A high-pressure stainless steel vessel (Nottingham, UK) was used to incorporate MER into γ-CD. Using a 1:1 mol ratio (0.07 mM) of the MER to γ-CD, MER (30 mg) and γ-CD (90 mg) were added into the vessel in the presence of 1 mL of water as cosolvent. After that, liquid CO_2 was pumped into the vessel using a syringe pump (Nottingham, UK) with a pressure of 60 bar. The vessel was placed in an ice bath to maintain its temperature at 6–8 °C. The stirring rate of 200 rpm with an entrainment paddle (Parr Systems, USA) was controlled using an overhead stirrer fitted in the vessel top. At the end of the experiment, the system was slowly depressurized and this pressure drop was responsible to change liquid CO_2 into CO_2 gas, which was released back into the air. The inclusion complex was later collected, washed with diethyl ether and, stored at 4 °C until further analysis (Scheme 1).

2.6. Preparation of MER-γ-CD loaded PLGA nanoparticles (MER-γ-CD NPs)

MER-γ-CD NPs were prepared using PLGA and MER-γ-CD by water/oil/water (W/O/W) emulsion solvent evaporation method with slight modifications (Guo et al., 2017). Briefly, 3 mL of the aqueous solution containing MER-γ-CD (50 mg, corresponding to 10.95 mg MER) was added slowly into 7 mL of 1% w/*v* PLGA solution (70 mg of PLGA into 7 mL of DCM) and sonicated for 3 min at 40 W in an iced water bath with a 5 sec on/off cycle to form uniform droplets by using a probe sonicator (Vibra Cell™ Sonicator). This primary emulsion (W/O) was added into MER-saturated PVA aqueous solution (2% w/v, 15 mL) with a glass syringe and sonicated for 5 min (10 sec on/off cycle) in an iced water bath to produce the final W/O/W emulsion. The final emulsion was left on the magnetic stirrer (4 °C) for overnight stirring to evaporate DCM.

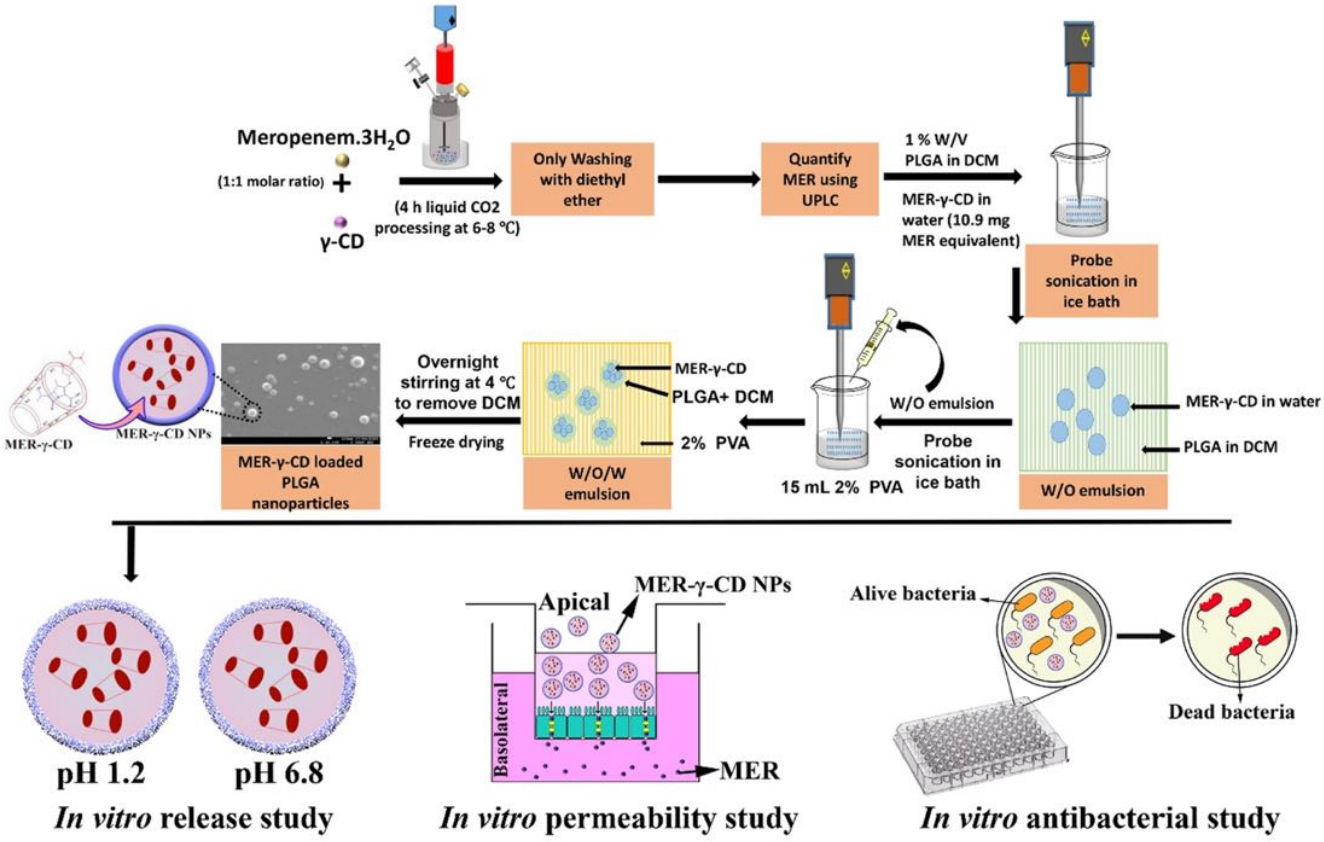

Scheme 1. Schematic illustration for the preparation of a novel delivery system of meropenem-in-cyclodextrin-in-PLGA nanoparticles and their systematic testing. First, MER was loaded into γ-CD using a novel Liquid CO_2 process. The setup includes a high-pressure stainless steel vessel maintained at a pressure of 60 bar using a syringe pump. The temperature of the vessel is maintained between 6 and 8 °C using an ice-bath and the overhead stirrer rotating at 200 rpm ensures homogenous loading of MER into γ-CD to make MER-γ-CD inclusion complex. Then, the MER-γ-CD inclusion complex was encapsulated into PLGA by the well-established double emulsion solvent evaporation method to make MER-γ-CD nanoparticles (NPs). Later, *in vitro* release study of MER-γ-CD NPs was performed in a universal buffer. Also, permeability studies were carried out using a Caco-2 monolayer culture model to analyze the transport of MER across the intestinal barrier. Lastly, the efficacy of the prepared oral MER formulations was carried out against *P. aeruginosa* and *S. aureus* using antibacterial assays.

Developed nanoparticles were collected by centrifuging (4 °C) the dispersion at 12,000 rpm (16,000 rcf) for 10 min and washing with water three times (Scheme 1).

Drug loading (DL) and Entrapment efficiency (EE) was calculated by measuring the unentrapped drug in the supernatant using UPLC analysis using equation (1) and (2).

$$DL\% = \frac{Weight\ of\ entrapped\ drug\ (Drug\ added - unentrapped\ drug)}{Weight\ (drug) + Weight\ (PLGA\ particles)} \times 100 \quad (1)$$

$$EE\% = \frac{Weight\ of\ entrapped\ drug}{Weight\ (drug\ added)} \times 100 \quad (2)$$

Cy5 loaded nanoparticles (Cy5-γ-CD NPs) were prepared as described above with the exception that 3 mg Cy5 was also dissolved into 3 mL of DCM with PLGA and 50 mg of γ-CD was used instead of MER-γ-CD.

2.7. Physicochemical characterization of MER-γ-CD complex and PLGA nanoparticles

2.7.1. Thermogravimetric analysis (TGA)/differential scanning calorimetry (DSC) studies

The thermograms for MER, γ-CD, PM, and MER-γ-CD inclusion complex were obtained using thermogravimetric analysis (TGA)/differential scanning calorimetry (DSC) instrument (Mettler Toledo, TGA/DSC, Columbus, OH, USA) was performed with a heating rate of 10 °C/min in an airy ambiance. Accurately weighed samples (3–5 mg) were placed in alumina crucibles and analyzed over a temperature range of 25–500 °C, and compared to a sealed empty alumina crucible maintained as a reference. The heating rate was maintained at 10 °C/min.

2.7.2. Powder X-ray diffraction (XRD) study

X-ray diffractograms and wide-angle XRD were recorded using a Bruker X-ray diffractometer (Bruker D8 Advance MKII XRD, Germany) with Cu radiation (λ = 1.54 Å). The samples were spread uniformly on a glass micro-sample holder and were analyzed over a 2θ range of 3–60° at a scanning rate of 2° (2θ) per min.

2.7.3. Fourier Transform- Infrared (FT-IR) spectroscopy

The FT-IR spectra were obtained using a Perkin Elmer ATR-FTIR Spectrometer. A small quantity of sample, enough to cover the diamond crystal, was used and the force gauge was set to 50. Number of scans were set to 254 and resolution was set to 16. The spectra for MER, MER-γ-CD, and the physical mixture of MER and γ-CD were measured for comparison.

2.7.4. Scanning electron microscopy (SEM)

For SEM images, a JEOL-JSM-7100F (Jeol, Japan) microscope was used at 10 kV. Sample preparation for SEM was performed in few steps, including (i) put the carbon tapes on aluminum stubs (ii) mount the empty silicon wafers on carbon tapes (iii) mount samples on silicon wafers and label them at the back of the stubs (iv) plasma cleaning (Evactron® 25, Japan) of samples for 10 mins (v) carbon coating [(Quorum Q150-TES, UK), 20 nm thickness)] of samples.

2.7.5. Proton nuclear magnetic resonance (^{1}H NMR) spectroscopy

The ^{1}H NMR study was performed using a Bruker AV 300 MHz spectrometer (Bruker Corporation, MA, USA). The chemical shifts were quoted as parts per million (ppm) downfield to the reference tetramethylsilane (TMS). All spectra were recorded by dissolving the samples in deuterium oxide (D_2O) as the solvent.

2.8. In silico molecular modeling studies

Computational studies were performed using the Schrödinger Small-Molecule Drug Discovery Suite (Schrödinger Release 2017-4: Schrödinger, LLC, New York, NY) on a Dell workstation running the 64 bit CentOS 6.9 Linux operating system with an eight-core Intel® Xeon 3.2 GHz processor; 32 GB RAM; 4 GB ASUS GTX 980 graphics card; 512 GB primary solid-state storage drive; and a 2 TB secondary storage hard disk drive.

2.8.1. Structure preparation

The two-dimensional chemical structure of MER was drawn using ChemDraw Professional (version 19.0) and then imported into Maestro. The LigPrep module was used to prepare the optimized three-dimensional structure of MER. This preparation includes the addition of explicit hydrogen atoms, generation of potential ionization states at pH 7.0 ± 2.0 using Epik, assessment of three-dimensional tautomers, and final energy minimization of the structure using the OPLS3 force field.

Meropenem contains two ionizable groups, a carboxylic acid (pKa 2.3) and a pyrrolidinyl amino group (pKa 7.4) (AstraZeneca). LigPrep yielded two MER structures, differing in the ionization of the amino group. Zwitterionic meropenem (MER-ZW) contained an anionic carboxylate group and a cationic pyrrolidinium group, whereas anionic meropenem (MER-A) contained the anionic carboxylate group and a unionized pyrrolidine group.

The crystal structure of γ-CD was acquired from a complex with maltodextrin binding protein MalE1 (PDB ID 5MKA). The complete crystal structure was imported from the Protein Data Bank (www.rcsb.org) into Maestro and then prepared using the Phase Protein Preparation Wizard. This preparation adds missing hydrogens, removes water molecules, optimizes hydrogen-bonding, and energy minimizes the structures using the OPLS3 force field. After preparation, γ-CD was separated from MalE1 in Maestro.

2.8.2. Molecular docking

A grid file for docking studies was created using the Glide module to position a 30 × 30 × 30 Å cube around the centroid of the γ-CD structure. This grid was used for Glide extra precision (XP) docking of the prepared meropenem structures.

2.8.3. Binding affinity prediction

The docked MER-ZW-γ-CD inclusion complex matched closely with the predicted inclusion complex from ^{1}H NMR studies and was investigated further to predict binding affinity using Prime MM-GBSA. This module estimates the binding free energy of the complex based on the change in the solvent-accessible surface area compared to the ligand and receptor alone. The Macromodel Embrace module was also used to predict binding free energy using two different methods: energy difference mode and interaction energy mode. The energy difference mode calculates the energies of the ligand, receptor, and complex separately and then determines the net change in energy. The interaction energy model predicts the binding energy based solely on the interactions of ligand and receptor.

2.8.4. Molecular dynamics

The docked MER-ZW-γ-CD inclusion complex was prepared for molecular dynamics (MD) using the **Desmond System Builder (Maestro-**Desmond Interoperability Tools, Schrödinger, New York, NY, 2017). The system was solvated using the TIP3P model, neutralized by adding sodium ions, and the ionic strength was set to 0.15 M using sodium and chloride ions. The OPLS3 force field was utilized for all calculations, and the system was relaxed using the default protocol. MD simulations were performed in the NPT ensemble at 300 K and 1.01325 bar pressure using Desmond Molecular Dynamics System (D.E. Shaw Research, New York, NY, 2017). Van der Waals and short-range electrostatic interactions

were cut off at 9 Å and the smooth particle mesh Ewald (PME) method was employed for the calculation of long-range electrostatic interactions. The reversible reference system propagation algorithm (RESPA) was used to integrate multiple time-step approaches, with a time step of 2 fs and long-range electrostatic interactions were computed every 6 fs. The temperature was controlled using a Nosé-Hoover chain thermostat, and the pressure using a Martyna-Tobias-Klein barostat. Simulations were performed for 5 ns each, with coordinates saved every 1.2 ps, and trajectories every 5 ps. These were analyzed using the integrated Simulation Interaction Diagram within SSMDDS and viewed in Maestro.

2.9. UHPLC method for MER

MER concentrations were determined using the UHPLC (Agilent 1290 Infinity, USA) method based on existing literature with slight modification (Mendez et al., 2003). Phosphate buffer was prepared by adjusting a solution of K_2HPO_4 (30 mM in distilled water) to pH 3 with orthophosphoric acid. Kinetex® C18 column was used (LC 250 × 4.6 mm, 5 µm (Phenomenex, USA) for quantification analysis. MER was eluted isocratically with mobile phase [30 mM phosphate buffer (A) / acetonitrile (B) at the ratio of 90/10%] at a flow rate of 0.7 mL/min, column temperature of 10 °C, 10 µL injection volume, and monitored with a UV detector at 220 nm. The concentration of MER was calculated using a standard calibration curve with a linear regression fitting factor (R^2) of 0.999.

2.10. In vitro drug release study

MER-γ-CD NPs (800 µg equivalent MER) were dispersed in 5 mL of universal buffer. Aqueous solutions of 0.05 M H_3PO_4 and 0.05 M CH_3COOH were mixed in a 1:1 (v/v) ratio to form a solution with a pH of 1.2. This solution was titrated at defined time points during the release experiment using 8 M NaOH to produce buffers with a pH of 6.8. MER-γ-CD NPs (800 µg MER equivalent), was dispersed into 5 mL of universal buffer (5 mL of a universal buffer with pH 1.2 contained 2.5 mL of 0.05 M H_3PO_4 and 2.5 mL of 0.05 M CH_3COOH) and stirred at 100 rpm at 37 °C under sink conditions. After 2 h, the pH was titrated to pH 6.8 by adding 25 µL of aqueous 8 M NaOH. Samples (200 µL) were withdrawn at predetermined time intervals and immediately replaced with an equal volume of fresh buffer solution of equivalent pH to maintain a constant volume. The withdrawn samples were centrifuged (14,000 rpm for 4 min) and run in UHPLC. The calculation of MER released from MER-γ-CD NPs was quantified with reference to a standard curve.

The possibility of using smaller sample sizes and smaller volumes of media offers many advantages in terms of material utilization. Therefore, the idea of small volume dissolution appeared recently that can serve as a valuable tool for dosage form screening or formulation selection in animals. Since there is no approved oral dosage form for MER we utilized this approach to make the process high throughput while keeping the drug at the detectable level using UPLC. Also, USP Apparatus 7 can accommodate a dissolution environment as low as 5 mL (Crist, 2009). Therefore, 5 mL of release media was used in this study.

2.11. In vitro biocompatibility of γ-CD and PLGA NPs

The potential cytotoxic effects of γ-CD and PLGA NPs on intestinal epithelial cancer cells (Caco-2, ATCC HTB-37, and LS174T cells, ATCC CL-188), were tested using the MTT assay. Caco-2 cells were cultured using DMEM (D5796) with 1% v/v each of sodium pyruvate, pen-strep, L-glutamine, MEM non-essential amino acids, and 10% FBS. LS174T cells were cultured in DMEM medium (D6546), containing 1% each of pen-strep and L-glutamine and 10% FBS. The cells were grown at 37 °C in a humidified incubator with 5% CO_2. Caco-2 cells (2×10^4 cells/ well), and LS174T cells (2×10^4 cells/well) were seeded into 96-well plates and grown for 24 h. The weighed masses of γ-CD and PLGA NPs (25, 50, 100, 250, 500, and 1000 µg/mL) were added to the media and incubated with cells for 24 h. Cells with medium only were used as negative controls and cells with solubilizing buffer (10% SDS in 0.1 N HCl) were used as positive controls for each plate. After incubation (24 h), the cell culture medium (with nanoparticles) was then aspirated and 100 µL/well of MTT reagent (0.5 mg/mL in PBS) was added for a further 4 h incubation at 37 °C. The formazan crystals were dissolved by adding 100 µL/well DMSO. The absorbance signal of formazan was measured at 570 nm using a microplate reader. Experiments were conducted with triplicate wells per treatment for each cell line and concentration.

2.12. Visualization of cellular uptake using laser scanning confocal microscopy

Caco-2 (2×10^5 cells/ well), and LS 174 T (4×10^5 cells/well) cells were seeded into Cellvis glass-bottom 12 well plate and grown for 24 h. Cy5-γ-CD NPs (100 µg/mL) prepared in the media was added to the plate and incubated for 4 h at 37 °C. Cells with medium only were used as control. After 4 h of incubation, the medium was removed, and the cells were washed thrice with chilled PBS (pH 7.4). Afterward, the cells were fixed with chilled 4% paraformaldehyde at room temperature for 20 min and washed thrice with chilled PBS with gentle rocking. Then cells were permeabilized with 0.2% Triton X-100 in PBS for 30 min and washed thrice with chilled PBS with gentle rocking. To block non-specific binding, cells were treated overnight with 1% BSA in PBS (2 mL) at 4 °C and then washed the cells once with PBS. Subsequently, the filamentous actin cytoskeleton of cells was stained with 1 mL of Phalloidin-FITC (stock concentration 50 mg/mL, then 1 µL from the stock into 1 mL of PBS for staining) for 20 min and washed thrice with chilled PBS to remove excess dye. Then 0.5 mL of DAPI (stock concentration 5 mg/mL, then 1 µL from the stock into 1 mL of chilled PBS for staining)) was used for nuclei staining for 10 min and cells were then washed three times with chilled PBS to remove excess DAPI. Before imaging, PBS was added to avoid dehydrating the samples and the dish was covered with Al-foil to protect the dye from light. Cell imaging was performed using a Laser Scanning Confocal Microscope Olympus FV3000 with a 60X objective lens immersed in oil. Phalloidin-FITC was used to label the cytoskeleton of the cell (λex-em 496–516 nm; green), and DAPI was used to label the cell nuclei (λex-em 358–461 nm; blue). The Cy-5 signals were recorded at λex-em 646–670 nm (red).

2.13. In vitro Caco-2 permeability experiments

The *in vitro* permeability of MER formulations were determined using the Caco-2 cell monolayer assay. Caco-2 cells (passage number P-9) were cultured in Phenol red-free DMEM medium (D8537) with 1% v/v each of sodium pyruvate, pen-strep, L-glutamine, MEM non-essential amino acids, and 10% of FBS and incubated under 37 °C with 5% CO_2. When reached 90% confluency, cells were trypsinized, harvested, and adjusted to cells density of 2×10^5/mL using fresh DMEM medium. Then, 0.5 mL cell suspension (1×10^5/mL) was seeded into the apical chamber (A) of 12 *trans*-well inserts (0.4 µm pore diameter, 1.12 cm^2 area) (Corning Inc., Kennebunk, ME, USA) plates. However, 1.5 mL of fresh medium was added into the basolateral chamber (B) of each insert.

2.13.1. Determination of TEER

First, the electrode of the EVOM volt-ohmmeter (World Precision Instruments, Sarasota, FL, USA) was pre-equilibrated in DMEM for 20 min. Meanwhile, the medium was changed from the transwell every second day, and 0.5 mL and 1.5 mL of fresh DMEM (pre-heated at 37 °C) were added to each well in A and B, respectively. After equilibrated at 37 °C for 20 min, Transepithelial Electrical Resistance (TEER) values were recorded. As a criterion, a monolayer with a Transepithelial Electrical Resistance (TEER) value ≥500 Ω.cm^2 was used for transport experiments (Kigen and Edwards, 2017). The TEER values of Caco-2 monolayers was measured and calculated as the equation below

$$\text{TEER}(\Omega.\text{cm}^2) = [\text{TEER}(\Omega) - \text{TEERbackground}(\Omega)] \times \text{A}(\text{cm}^2) \quad (3)$$

TEER (Ω) is the electrical resistance across Caco-2 monolayers, TEER background (Ω) is the resistance across the insert only without cells. A (cm^2) is the surface area of the insert, 1.12 cm^2.

2.13.2. Bi-directional transport experiment

In our experiment, Caco-2 cells with TEER ≥ 500 Ω.cm^2 were recorded within 6 days, which is an indicator of monolayer development. To investigate the permeability (A to B), the medium from each well was replaced with preheated HBSS (washing of monolayer) and equilibrated at 37 °C for 20 min. HBSS solution on both sides of the cell monolayer was removed by decanting (transwell insert) and aspiration (bottom of plate well). After that, the dosing (A) chamber was replaced with 500 μg/mL of MER alone or equivalent concentration of MER-γ-CD, and MER-γ-CD NPs in HBSS and 1.5 mL of HBBS only in receiving chamber (B). Efflux study (B to A) was performed similarly, however, the dosing and receiving sides were B and A, respectively. Plates were placed in a shaking incubator (John Morris Scientific, Australia) at 37 °C and 100 rpm to simulate the small intestine motility. In each study, samples (0.2 mL) were taken out from the receiving chamber after 3 and 6 h. The volume of the receiving chamber was maintained constant by replacing the withdrawn samples with a similar volume of HBSS.

The apparent permeability coefficient (P_{app}, cm/s) was determined according to the following equation.

$$P_{app} = (dQ/dt)/(C_0 \times A) \quad (4)$$

dQ/dt is the MER transport rate (ng/s), C_0 is the initial concentration of MER on the dosing chamber (ng/mL). A is the surface area of inserts (1.12 cm^2).

The efflux ratio (ER) was determined using following equation:

$$ER = P_{app}(B \rightarrow A)/Papp(A \rightarrow B) \quad (5)$$

Papp (B → A) and Papp (A → B) are representing the apparent permeability of tested formulations.

2.14. In vitro antibacterial assay

Broth microdilution method was used to determine the minimum inhibitory concentration (MIC_{90}) of antimicrobial agent that inhibits visible growth of a microorganism such as *P. aeruginosa* (ATCC 27853 and clinical strain 23) and *S. aureus* (ATCC 29213 and clinical strain 54) according to the procedure established by the European Committee on Antimicrobial Susceptibility Testing (EUCAST) (2019). Briefly, serial two-fold dilutions of antibiotic samples such as MER, MER-γ-CD, and MER-γ-CD NPs (concentrations of MER in formulations is equivalent ranged from 0.0313 mg/L to 16 mg /L) were prepared in CAMHB (cation adjusted Mueller Hinton Broth) and aliquoted (100 μL) into flat-bottom microtiter plates. McFarland 0.5 standardized inoculum suspension (1 × 10^6 CFU/mL) prepared in sterile distilled water was added into cation adjusted Mueller Hinton Broth (CAMHB) to give rise to approximately 1 × 10^6 CFU/mL. Then 100 μL of inoculum suspension prepared in CAMHB was added to the drug samples containing microtiter plates to give rise to approximately 5 × 10^5 CFU/mL. After that, inoculated plates were incubated at 37 °C for 16 to 20 h and MIC_{90} values were determined spectrophotometrically at 620 nm. This experiment for the determination of MIC_{90} values was repeated three times.

3. Statistical analysis

All experiments were performed in triplicate except where otherwise stated so that one-way ANOVA and post-hoc Tukey's tests could be applied to analyze the data.

4. Results and discussions

4.1. MER solubility in liquid CO_2

MER solubility was investigated in a cold process (under 8 °C), a liquid CO_2 method. Solubility data of MER in liquid CO_2 is shown in Fig. 1. The mass of MER (mg) dissolved in liquid CO_2 is plotted against time (h). A thin solid layer of MER attached to the wall of a high-pressure SS vessel showed that MER was solubilized during processing and recrystallized on the wall during decompression. The results showed that the solubility of MER in liquid CO_2 reached saturation after 12 h (~8.9 mg/60 mL) indicating MER is slightly soluble in CO_2 (14 mg/100 mL) at the conditions specified (6–8 °C, 60 bar). The solubility of MER after 15 and 18 h was similar to that obtained after 12 h. It is worth to note that there was no colour change in liquid CO_2 processed MER (**Figure S2, Supporting Information**). Later, we also run another experiment (**d**), where the solubility of MER (30 mg) was determined in liquid CO_2 in the presence of cosolvent; water (1 mL). It was worth noting that MER was completely dissolved in the presence of cosolvent.

4.2. Solid-state characterization of MER processed in liquid CO_2

4.2.1. FTIR

The FTIR spectra of the commercial and liquid CO_2 processed MER showed characteristic bands at similar positions (Fig. 2**a**). MER displayed broad bands at 3568 cm^{-1} and 3401 cm^{-1} that are attributed to —OH and —NH stretching, respectively. A sharp band at 1748 cm^{-1} corresponds to C═O stretching in COOH. Other bands at 1188 cm^{-1} and 668 cm^{-1} are ascribed to —CN stretching in pyrrolidine ring and —OH bending in COOH, respectively.

4.2.2. X-Ray diffraction

The XRD spectra of both commercial and liquid CO_2 processed MER showing peak intensities at 2θ of 12.74, 16.85, and 25.49, etc. were overlapped on each other (**Figure b**). This shows that both samples are crystalline.

4.2.3. Thermoanalysis

DSC thermograms of commercial and liquid CO_2-processed MER are shown in (Fig. 2**c**). The water desorption (110 °C) and melting point peaks (186 °C) overlapped with each other and showed no change, indicating that no polymorphism was observed in the commercially

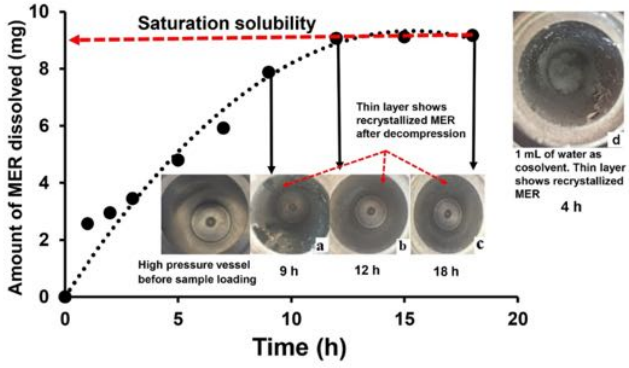

Fig. 1. Saturation solubility curve of MER in liquid CO_2 at 60 bar and 6–8 °C (n = 10). This data explained that the thickness of the thin layer of recrystallized MER in the vessel increases over time up until (b) 12 h and (c) 18 h. The black dotted curve is the best fit line ($y = -0.0396x^2 + 1.2159x$) and the red dashed line is saturation solubility. Each data point is obtained from 10 separate experiments. A single experiment was also performed to find the solubility of MER (30 mg) in liquid CO_2 in the presence of cosolvent; water (1 mL) for 4 h, showing that meropenem was completely dissolved in the presence of cosolvent.

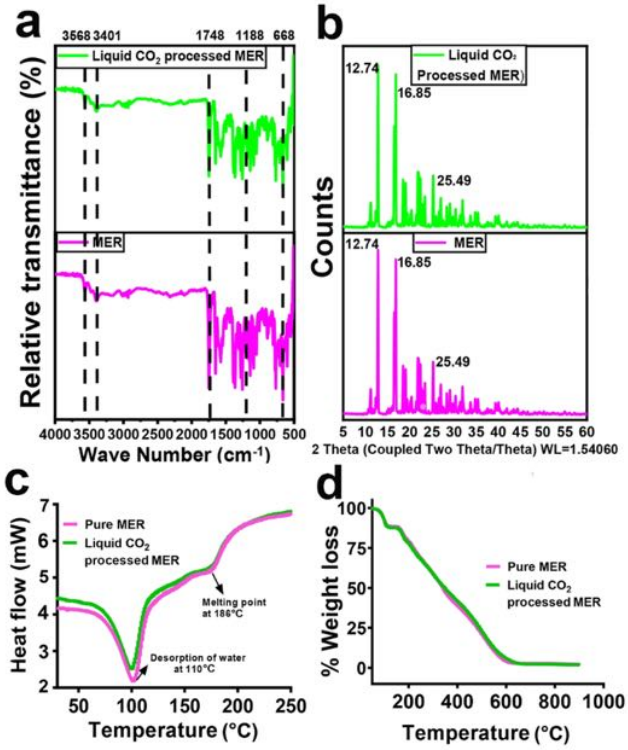

Fig. 2. Fourier Transform Infrared (FTIR) Spectra of commercial MER compared with liquid CO_2 **(a)** processed MER, showing that MER was stable in liquid CO_2. X-ray diffraction (XRD) spectra of commercial MER compared with liquid CO_2 **(b)** processed MER, confirming that liquid CO_2 processed MER was stable with its crystalline peaks, DSC (**c**) and TGA (**d**) thermograms of commercial MER compared with liquid CO_2 processed MER further confirmed that MER was stable in the cold process.

available form of MER. Also, the TGA thermograms (Fig. 2**fd** confirmed no change in the polymorphic state of commercially available form of MER after processing with liquid CO_2.

4.2.4. UPLC analysis

The UPLC data (**Figure S3, Supporting Information**) for commercial MER and liquid CO_2 processed MER, showing retention time at 9.6 min. All these results showed that the cold liquid CO_2 method is suitable for MER loading into different nano-carriers.

4.3. Job's plot reveals the stoichiometry of the host-guest inclusion complex

One of the best methods used to recognize the stoichiometry of the host-guest inclusion complexes is Job's method, also known as the continuous variation method (Job, 1928), which has been applied here by using UV–visible spectroscopy. A series of solutions (0–30 μM) for MER and γ-CD were prepared with their different mole fractions in the range 0–1 (**Tables S1, Supporting information**). In the present work, the maximum value of change in ultraviolet absorption was found at R = 0.5, which suggests 1:1 stoichiometry of the MER-γ-CD (**Figure S4a, Supporting Information**).

Moreover, the effects of γ-CD on the UV–vis absorption spectra of MER are illustrated in **Figure S4b (Supporting Information)**. The absorption spectra of MER (0.1 mM) showed an obvious decrease in the absorbance with increasing the concentration of γ-CD (0.2–0.5 mM). Due to the inclusion of MER by the γ-CD cavity, the substituent or conjugated structure of the electron delocalization was restricted, which led to the decrease in the absorbance (Huang et al., 2017; Yáñez et al., 2012).

4.4. Preparation and characterization of MER-γ-CD inclusion complex

Drug loading and encapsulation efficiency are the two most important parameters for evaluating the quality of the preparation method and its product such as the inclusion complex. The results of these two parameters for MER-γ-CD as prepared by the liquid CO_2 method are shown in **Table S2 (Supporting Information)**. The inclusion complex obtained via the liquid CO_2 method gave higher drug loading (21.9%) and encapsulation efficiency (92.2%) values, which confirms the efficiency of our method.

4.4.1. FT-IR analysis

The FTIR spectra of MER, γ-CD, physical mixture (PM), and MER-γ-CD are presented in Fig. 3**a**. The IR spectrum of MER displayed broad bands at 3568 cm^{-1} and 3401 cm^{-1} that are attributed to —OH and —NH stretching, respectively. A sharp peak at 1750 cm^{-1} corresponds to C═O stretching in COOH. Other peaks at 1188 cm^{-1} and 668 cm^{-1} are ascribed to —CN stretching in pyrrolidine ring and —OH bending in COOH, respectively. The FT-IR spectrum of γ-CD exhibited characteristic bands at 3305 cm^{-1} (O—H stretching vibration), 2917 cm^{-1} (C—H stretching vibration), 1633 cm^{-1} (H—O—H bending), and 1020 cm^{-1} (C—O—C stretching vibration) (Xiao et al., 2014). The spectrum of the physical mixture (PM) showed less intense bands of MER (1750 cm^{-1}) and γ-CD (1633 cm^{-1} and 1020 cm^{-1}) demonstrated some interaction between MER and γ-CD during the formation of PM. However, the FT-IR spectrum of MER-γ-CD complex clearly showed that characteristic peaks of MER are disappeared or some less intense peaks are observed at 1750 cm^{-1}, and 1188 cm^{-1}. These results depicted that some functional groups of MER are included in the cavity of γ-CD to form a molecular complex.

4.4.2. XRD

Powder XRD (P-XRD) studies were performed to detect the crystallinity of the pure drug and inclusion complex. As shown in Fig. 3**b**, MER (2θ = 12.74, 16.85 and 25.49°) and γ-CD (2θ = 7.9, 15.4, and 22.2°) exhibited several intense and sharp peaks, which confirm their crystalline nature. XRD spectrum of PM was equivalent to the simple combination of MER and γ-CD, where fewer sharp peaks of both MER and γ-CD were observed. However, XRD spectra of the MER-γ-CD inclusion complex showed that no sharp peaks are corresponding to the MER and γ-CD, which depicted that MER might be incorporated in the cavity of γ-CD and changed to the amorphous state during the complexation process.

4.4.3. Thermogravimetric analysis (TGA)/differential scanning calorimetry (DSC) studies

The thermal properties of the MER-γ-CD inclusion complex were investigated by-TGA and DSC methods. A systematic analysis of the TGA curves (**Figure S5a, Supporting Information**) showed that 50% of MER decomposes at 338 °C. However, the thermal stability of the inclusion complex was different; that is, 50% of the MER-γ-CD inclusion complex was decomposed at 404 °C, showing that MER is more stable when incorporated into γ-CD. The DSC thermogram gave further information about the thermal properties of the MER-γ-CD inclusion complex. As shown in **Figure S5b (Supporting Information)**, the DSC curve of MER has sharp peaks at 110 °C (water desorption) and 186 °C (melting point). However, in the DSC curve of MER-γ-CD, both sharp peaks disappeared, predicting the incorporation of MER into the γ-CD cavity.

4.4.4. SEM analysis

The SEM images of MER, γ-CD, PM, and MER-γ-CD inclusion complex are shown in Fig. 4**.** Pure MER (Fig. 4**a**) existed as irregularly shaped crystals, whereas γ-CD (Fig. 4**b**) crystallized as bulk crystals. The physical mixture of MER/ γ-CD (Fig. 4**c**) revealed both crystalline components. In contrast, the inclusion complex (Fig. 4**d**) appeared as irregular particles, in which the original morphology of both

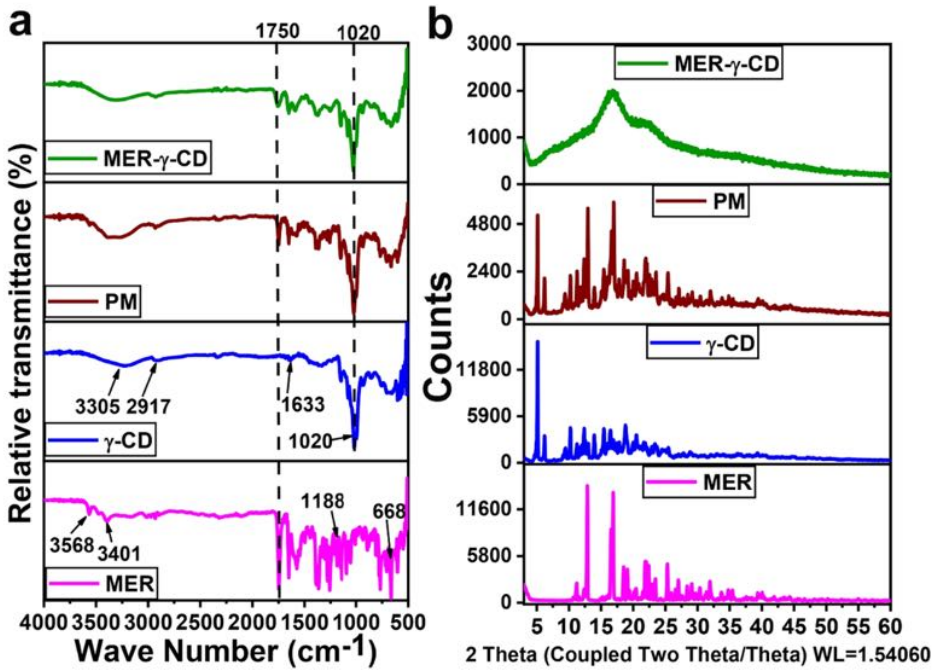

Fig. 3. **(a)** FTIR spectra of MER, γ-CD, PM and MER, γ-CD inclusion complex. The results showing that some functional groups of MER are included in the cavity of γ-CD to form a molecular complex. **(b)** XRD spectra of MER, γ-CD, PM, and MER, γ-CD inclusion complex It showed that MER might be incorporated in the cavity of γ-CD and changed to the amorphous state during the complexation process.

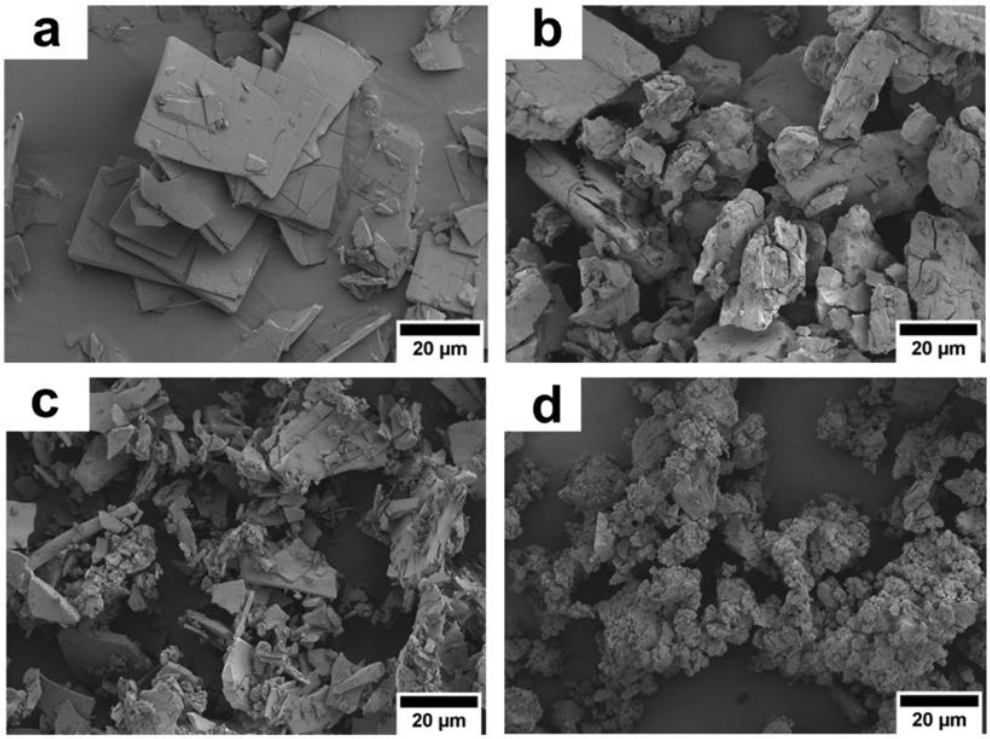

Fig. 4. SEM images for MER (**a**), γ-CD (**b**), PM (**c**) and MER, γ-CD inclusion complex (**d**). It showed that MER and γ-CD have existed in sharp and bulk crystals, respectively. However, when solutions of MER and γ-CD were mixed, a close association resulted in the inclusion complex, where MER and γ-CD have no longer existed in its crystalline state.

components disappeared and tiny aggregates of amorphous, irregular-sized pieces were present. These images further demonstrated that, when the powders of MER and γ-CD were simply mixed physically, they continued to exist in their original, individual forms, whereas, when the solutions of the two compounds were mixed, they formed a close association, probably forming the inclusion complex, in which MER and γ-CD have no longer existed in its crystalline state.

4.4.5. ^{1}H NMR spectra analysis

The molecular interaction of host-guest molecules in inclusion

complexes is most commonly investigated using ^{1}H NMR (Singh et al., 2010). Normally, ^{1}H NMR is used to obtain information regarding chemical shift displacement of host and guest molecules. These chemical shifts are easily observed for protons located at the inner surface (H-3 and H-5), and the outer surface (H-1, H-2, H-4, H-6) of the CDs. It was observed that the chemical shift displacements were the changes in the chemical shifts due to complexation and not because of the non-specific correlation between host-guest molecules (Butkus et al., 1996).

The possible interaction mode between MER and γ-CD for inclusion complex formation was investigated by comparing the ^{1}H NMR spectra of MER, γ-CD, and the MER-γ-CD inclusion complex in D_2O (**Figure S6, Supporting Information**). The chemical shifts of γ-CD protons with or without MER are compared in **Table S3a (Supporting Information)**. The chemical shift variations were calculated by the equation:

$$\Delta\delta = \delta(\text{complex}) - \delta(\text{free}) \quad (6)$$

The positive and negative signs represented a downfield and upfield shift, respectively. In **Table S3a (Supporting Information)**, evident upfield shifts (−0.007 and −0.002 ppm) could be observed for the H-3 and H-5 protons that are located inside the cavity of γ-CD. But comparatively smaller shifts of H-2 and H-4 protons (0.003 and −0.002 ppm) could be observed that are located outside the cavity. These findings could represent the correlation between the guest molecule and the interior of the host cavity. It is known that H-5 protons are near the narrow side while H-3 protons are near the wide side of the cavity of γ-CD, as shown in **Figure S5f (Supporting Information)**. In our study of inclusion complex formation, H-3 possessed a larger chemical shift variation (−0.007 ppm) than H-5 (−0.002 ppm). So it could be proposed that MER was inserted from the wide side of the γ-CD cavity (Yang et al., 2011). Moreover, the H-3 and H-5 protons are masked with dense electronic clouds; this cloud shields the protons and results in upfield shifts (Tang et al., 2015).

The inclusion mode of the MER-γ-CD was further investigated by comparing the ^{1}H NMR spectrum of MER in the absence and presence of γ-CD. As illustrated in **Figure S6c (Supporting Information)**, mostly MER signals appeared at 1.121–4.702 ppm, which were probably similar to the γ-CD protons (3.481–5.040 ppm). Therefore, a lot of MER proton signals overlapped in the spectra of the MER-γ-CD complex (**Figure S6e, Supporting Information**). It was observed that MER proton signals were weaker as compared to γ-CD due to the less percentage of MER in the inclusion complex. Moreover, γ-CD induced chemical shift changes were also reported for MER protons signals between the free and complexed state (**Table S3b, Supporting Information**). From **Table S3b (Supporting Information**, we can see that γ-CD induced variations occurred in most of the protons such as H-2 (pyrrolidine ring), H-14 (β-lactam ringside), and H-15 (pyrolline ring). These findings proposed that β-lactam, pyrolline, and pyrrolidine ring (partially) sides of MER were deeply penetrated into the cavity of γ-CD. The possible inclusion mode for the MER-γ-CD inclusion complex is demonstrated in **Figure S6f (Supporting Information)**.

4.5. *In silico MER-γ-CD docking*

4.5.1. *Molecular docking*

The three-dimensional structures of MER-ZW (Fig. 5**a**) and MER-A (**Figure S7a, Supporting Information**) were docked into γ-CD using Glide XP docking. Both structures were predicted to form favorable inclusion complexes based on the XP Glide score (MER-ZW: −2.851, MER-A: −2.875). The docking pose of MER-ZW in γ-CD (Fig. 5**B**) closely matched the proposed inclusion complex from the ^{1}H NMR studies (**Figure S5f**). This binding pose predicts MER-ZW to have two hydrogen-bond interactions with hydroxyethyl groups of γ-CD: the hydroxyethyl tail of MER-ZW as a hydrogen-bond donor, and the beta-lactam carbonyl group. The docking pose of MER-A in γ-CD is also available in **Supporting information (Figure S7)**

4.5.2. *Binding affinity predictions*

The binding affinities of the Glide XP docked inclusion complexes were predicted using three different methods (**Table S4, Supporting Information**). Prime MM-GBSA calculates binding affinity based on the net difference in the solvent-accessible surface area between the inclusion complex and meropenem and γ-CD separately. The MER-A-γ-CD complex is predicted to have a slightly stronger binding with γ-CD compared to the MER-ZW-γ-CD (-45.141 kcal/mol vs −37.731 kcal/mol). The majority of this energy results from Coulomb and Van der Waals energy, followed by lipophilic energy.

The MacroModel Embrace module was also used to predict binding free energy using two different modes. Energy difference mode calculates the net difference in energy between the inclusion complex and individual components of the system. Interestingly this mode predicted

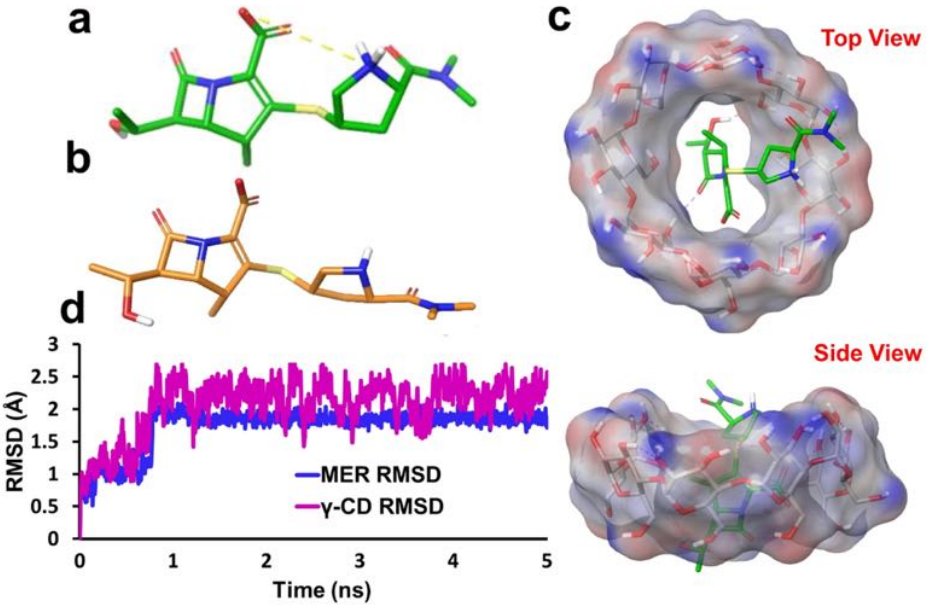

Fig. 5. LigPrep three-dimensional structure of MER-ZW (**a**) and MER-A (**b**). (**c**) Top and side views of the Glide XP docked MER complex with γ-CD (grey with the electrostatic potential surface). A purple dashed lines indicate hydrogen bonds. (**d**) RMSD of MER-ZW and γ-CD over a 5 ns MS simulation.

MER-ZW to have stronger binding than MER-A (-77.915 kcal/mol compared to −65.564 kcal/mol). This was primarily due to the difference in predicted electrostatic energy of the MER-ZW inclusion complex (-177.045 kcal/mol compared to −96.247 kcal/mol for MER-A). The interaction energy mode of MacroModel Embrace calculates binding free energy solely from the interactions of the inclusion complex. This mode predicted a slightly stronger binding of MER-A with γ-CD than MER-ZW (−352 kcal/mol compared to −339 kcal/mol).

4.5.3. Molecular dynamics simulations

To analyze the stability of the docked MER-ZW-γ-CD inclusion complex, the predicted binding pose was entered into a 5 ns MD simulation. MD solvates the inclusion complex system, simulating solvent interactions, and also the transfer of energy and subsequent positional changes across the entire system. The RMSD of the MER-ZW and γ-CD structures were tracked over the MD simulation, showing an initial change in pose to form a more stable inclusion complex, as indicated by the low fluctuation in RMSD after approximately 1 ns of simulation (Fig. 5**c**). Comparatively, MER-A was less stable and the γ-CD did not stabilize over the simulation **(Figure S7b, Supporting Information).**

4.6. Characterization of MER-γ-CD loaded PLGA nanoparticles (MER-γ-CD NPs)

MER-γ-CD NPs were prepared using a double emulsion solvent evaporation method. The FTIR spectra of MER, γ-CD, PLGA NPs, and MER-γ-CD NPs are presented in **Figure S8 (Supporting Information)**. The IR spectra of MER and γ-CD with their characteristic bands is explained in inclusion complex section. The FTIR spectrum of PLGA NPs showed characteristic band at 1753 cm^{-1} (C═O) (Basu et al., 2016). However, the spectrum of MER-γ-CD NPs clearly showed that characteristic peaks of MER and γ-CD are disappeared or some less intense peaks are observed, confirming the interaction or loading of inclusion complex into PLGA NPs.

The average size of PLGA NPs and MER-γ-CD NPs from SEM was 190.4 nm and 216.2 nm, respectively **(**Fig. 6**a, b)**. The hydrodynamic size of PLGA NPs was 164.2 nm, which was increased to 220.2 nm in the case of MER-γ-CD NPs **(**Fig. 6**c, Table S2, Supporting Information)**. The zeta potential of PLGA NPs and MER-γ-CD NPs was noticed at −22.3 and −22.8, respectively **(**Fig. 6**d, Table S2, Supporting Information).**

Drug loading and entrapment efficiency of the MER-γ-CD NPs were observed as 3.6% and 42.1%, respectively **(Table S2, Supporting Information)**. Similar findings have been reported earlier, where drug loading and entrapment efficiency of drugs is very low with PLGA NPs (Kashi et al., 2012; Vaidya et al., 2019). Moreover, it was also confirmed that the major drawback of loading hydrophilic drugs into PLGA NPs is their low drug loading and entrapment efficiency (Govender et al., 1999; Kashi et al., 2012). Another reason for the low drug loading of hydrophilic drugs is to rapidly diffuse to the external aqueous phase (Govender et al., 1999). Therefore, we saturated the external aqueous phase with MER first to minimize the diffusion of the drug.

4.7. In vitro drug release study

A universal buffer was used to evaluate the drug release profile from MER-γ-CD NPs at 37 °C. In the first 2 h, the amount of active and total drug release was 5.1 and 7.6% in simulated gastric pH (1.2), respectively. After that, pH was changed into simulated intestinal pH (6.8). There was 23.6 and 27.4% of active and total drug (MER) released from MER-γ-CD NPs within 8 h (Fig. 6**e**). It is important to note here that this experiment was performed with a universal buffer, where the impact of physiological parameters on nanoparticle degradation and drug release could not be seen, which is more likely to happen in an actual intracellular environment.

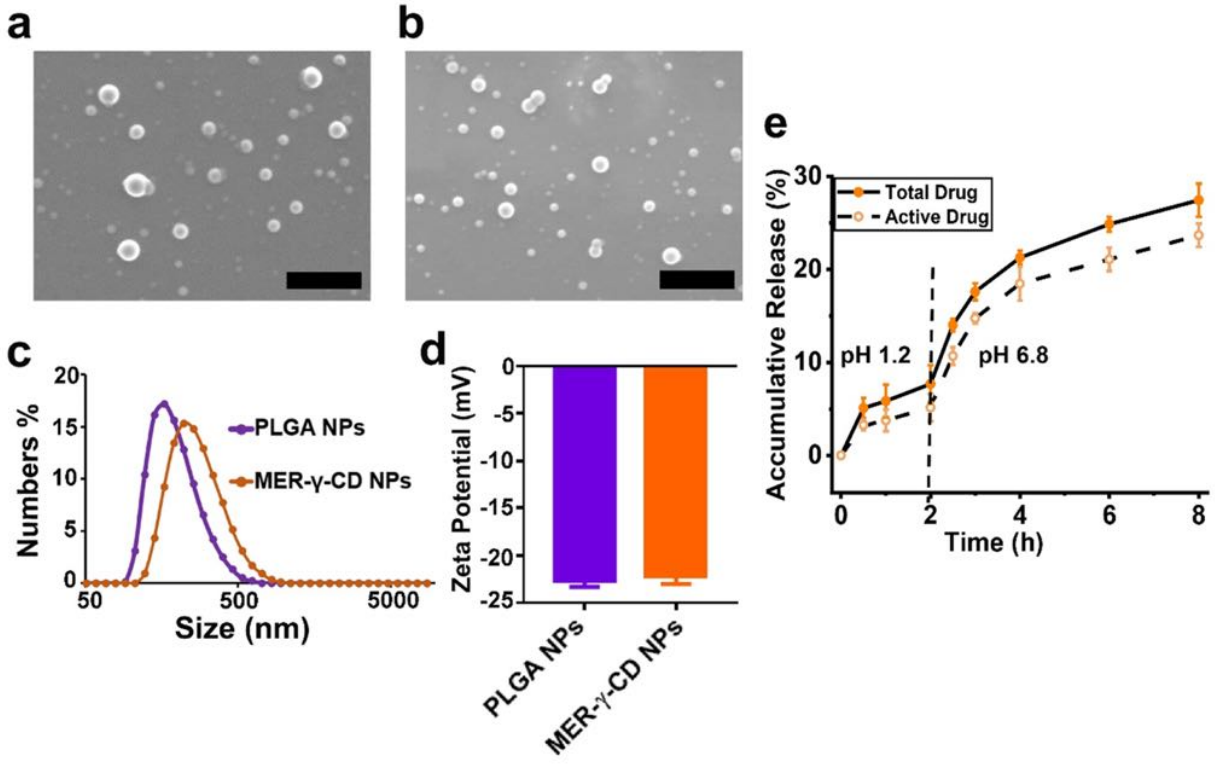

Fig. 6. SEM images for PLGA NPs (**a**) and MER-γ-CD NPs (scale bar = 1 μm) (**b**). (**c**) DLS hydrodynamic diameter of particles analyzed by suspending in water. **(d)** Zeta potential of the particles measured using DLS. (**e**) MER release profile from MER-γ-CD NPs particles in the universal buffer (gastric pH for 2 h, intestinal pH for 6 h) at 37 °C. In the first 2 h, the amount of active and total drug release was 5.1 and 7.6% in simulated gastric pH, respectively. Thus, 23.6 and 27.4% of active and total drug (MER) was released from MER-γ-CD NPs in 8 h, respectively (n = 3 ± SD).

4.8. In vitro biocompatibility of γ-CD and PLGA NPs

In this assay, two intestinal epithelial adenocarcinoma cell lines (enterocyte-like Caco-2 and goblet cell-like LS174T) were used to evaluate the *in vitro* biocompatibility and cytotoxicity of γ-CD and PLGA NPs. To investigate it, these cells were treated with six different concentrations (25–1000 μg/mL) of γ-CD and PLGA NPs for an incubation time of 24 h. As seen from **Figure S9 (Supporting Information)**, at higher concentrations (250–1000 μg/mL), PLGA NPs were found to be significantly cytotoxic in LS174T and Caco-2 cells. However, no significant cytotoxicity for γ-CD was observed in both cell lines at any concentration, which was found more biocompatible as compared to PLGA NPs.

4.9. Determining intracellular uptake using laser scanning confocal microscopy

Cellular internalization of the drugs via different carriers such as nanoparticles is a promising strategy to enhance their therapeutic efficacy. To investigate this phenomenon, we loaded PLGA NPs with Cy5 dye to make them fluorescent (red color). Briefly, Cy5-γ-CD NPs were incubated for 4 h with intestinal cancer cells (Caco-2 and LS174T). After cell fixation, fluorescent reagent such as DAPI (blue color) and phalloidin-FITC (green color) was used to visualize the nucleus and cytoskeleton of the cells, respectively. To confirm whether Cy5-γ-CD NPs are internalized or simply adsorbed onto the surface of cells, images for all cell types were taken at multiple confocal depths (z-sections) using confocal microscopy. As depicted in **Figure S10 (Supporting Information)**, red fluorescent particles were observed to be distributed in the cytoplasm of all cell types tested here, indicating that our particles could have the potential to carry any drug to internalized into the cells.

4.10. In vitro permeability assay

To predict the permeability profile of MER, MER-γ-CD inclusion complex, and MER-γ-CD NPs, the Caco-2 monolayer culture model was used because it is known for both absorptive (A to B) and secretory (B to A) characteristics of epithelial intestinal cells. Therefore, the bidirectional transport of MER and its formulations (MER equivalent concentration of 500 μg) was performed across the Caco-2 monolayer at different time points (3 and 6 h). As shown in Fig. 7**a, b**, and MER-γ-CD inclusion complex and MER-γ-CD NPs were observed to have similar absorptive and secretory transport of MER as compared to MER solution at different time points of 3 and 6 h.

According to Fig. 7**c**, the apparent permeability coefficient (Papp) (A to B) values are 2.63×10^{-6} cm/s, 2.81×10^{-6} cm/s, and 2.92×10^{-6} cm/s for MER, MER-γ-CD inclusion complex, and MER-γ-CD NPs, respectively. For secretory transport, the Papp (B to A) values were 1.47

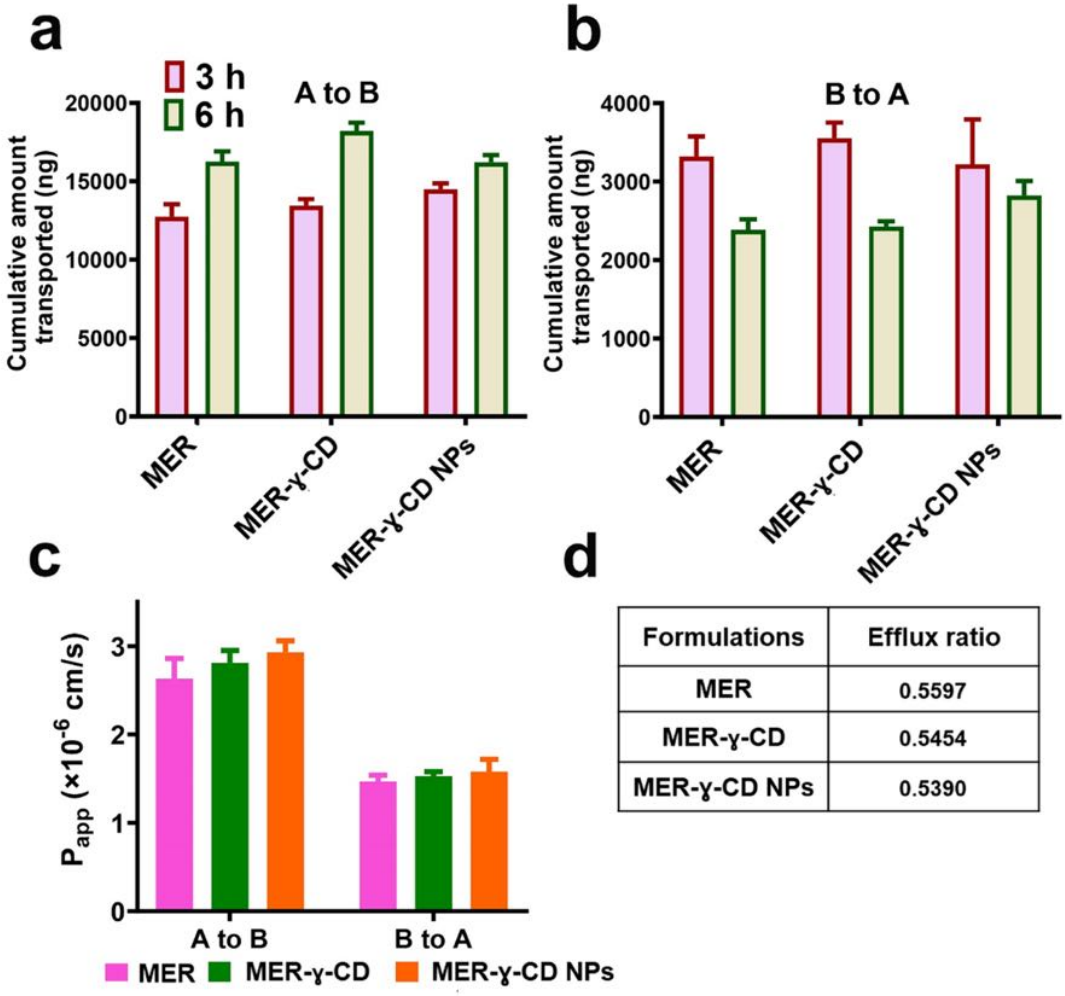

Formulations	Efflux ratio
MER	0.5597
MER-γ-CD	0.5454
MER-γ-CD NPs	0.5390

Fig. 7. The cumulative amount of MER transported **(a)** A to B and **(b)** B to A through the Caco-2 monolayer at 3 and 6 h, where monolayers were incubated with MER, MER-γ-CD inclusion complex, and MER-γ-CD NPs (MER equivalent concentration of 500 μg/mL) (all data are n = 3, mean ± SD) (c) Apparent permeability coefficient (Papp) of MER from MER-γ-CD inclusion complex and MER-γ-CD NPs at 6 h in the Caco-2 monolayer (all data are n = 3, mean ± SD (d) Efflux Ratio for MER, MER, MER-γ-CD inclusion complex and MER-γ-CD NPs. Non-significant data.

$\times 10^{-6}$ cm/s, 1.53×10^{-6} cm/s, and 1.58×10^{-6} cm/s for MER, MER-γ-CD inclusion complex and MER-γ-CD NPs, respectively. It is reported in different studies that drugs with Papp $> 10^{-6}$ cm/s presented excellent oral bioavailability (Artursson et al., 2001; Bergeon et al., 2010), therefore all our formulations could be a suitable candidate for further oral drug absorption evaluation. Also, the efflux ratio (ER) values (Fig. 7**d**) were 0.55, 0.53, and 0.54 for MER, MER-γ-CD inclusion complex, and MER-γ-CD NPs, respectively, indicating no effect of our drug carriers on the efflux of MER. The results also showed that the permeability of each formulation was high even there was no significant contribution from the carriers to enhance the permeability as expected. It is important to note that the permeability of drugs from the Caco-2 monolayer may dependent on the passage number of Caco-2 cells and drug concentration. It is well known that the expression of P-gp protein is not well established in Caco-2 cells with lower passage number (Shirasaka et al., 2008). Moreover, a study also shows that A to B permeability of drugs increased when A concentration was increased, showing a sigmoid-type relationship to donor (A) concentrations. Further, at a higher concentration range, permeability reached a maximum value, suggesting saturation of P-gp-mediated efflux, and at the lower concentration range, permeability decreased depending on P-gp expression level (Shirasaka et al., 2008).

Next, a recovery experiment based on TEER values was performed to evaluate the integrity of the Caco-2 monolayer. After 6 h of permeability experiment, the monolayer was washed thrice with DMEM media to remove any particle on the Caco-2 monolayer. TEER values were noted at different time points (0, 6, 10, 14, and 24 h). **Figure S11 (Supporting Information)** illustrates that the integrity of the Caco-2 monolayer was recovered within 24 h, confirming the transient decrease of TEER was due to permeation of drug across cell monolayer via tight junctions (Lamson et al., 2020).

4.11. In vitro antibacterial activity

The minimum inhibitory concentration (MIC_{90}) of MER-loaded particles was investigated using broth micro-dilution followed by EUCAST guidelines. We used both gram-positive (S. aureus) and gram-negative (*P. aeruginosa*) species of bacteria to determine the antibacterial effect of MER formulations. According to EUCAST guidelines, the MIC_{90} range of MER against ATCC strains of *P. aeruginosa* and *S. aureus* are 0.125–1 mg/L (2020) and 0.03–0.12 mg/mL (2010), respectively. As summarized in Table 1, MIC_{90} values for MER free drug against reference and clinical strains of *P. aeruginosa* are 0.25 mg/L. However, MER-γ-CD showed half of the MIC_{90} (0.125 mg/L) against reference strains of P. aeruginosa as compared to free MER. In the case of MER-γ-CD NPs, MIC_{90} values against reference and clinical strains of *P. aeruginosa* are 0.125 and 0.25 mg/L, respectively. For ATCC and clinical strains of *S. aureus*, the MIC_{90} values of free MER are 0.0625 mg/L. For the MER-γ-CD inclusion complex, MIC_{90} values are similar to free drug against the ATCC strain but half of the free drug against the clinical strain of *S. aureus*. However, half of the MIC values of MER-γ-CD NPs were noticed against the clinical strain of *S. aureus* as compared to free MER. Our formulations showed the potential to significantly decrease the MIC_{90} values of the Pure MER. It has been reported that adsorbed antibiotics on nanoparticles are more effective than antibiotics in solution because antibiotic-loaded nanoparticles could act on the bacteria with high local antibiotic concentration, which led to perforation of the bacterial cell membrane (Azad et al., 2013; Weinstein and Lewis, 2020). However, based on EUCAST guidelines, the MIC values against all bacterial strains were within the range of free drug, concluding that our formulations were able to retain the antibacterial activity.

Table 1
Values of MIC_{90} (mg/L) of MER and MER loaded particles against ATCC and clinical isolates of selected Gram-negative (***P. aeruginosa) and*** Gram-positive bacteria (***S. aureus)***.

Formulations	*P. aeruginosa* (mg/L)		*S. aureus* (mg/L)	
	ATCC	Clinical strain 23	ATCC	Clinical strain 54
MER	0.25	0.25	0.0625	0.0625
MER-γ-CD	0.25	0.125	0.0625	0.0313
MER-γ-CD NPs	0.125	0.25	0.0313	0.0313

5. Conclusion

The present study aimed to (i) determine the saturation solubility of MER in liquid CO_2, (ii) loading of MER into γ-CD, and then into PLGA NPs (iii) protecting MER at gastric pH and (iv) increasing the intestinal permeability and bioavailability. In summary, MER was successfully incorporated into γ-CD using a cold process (liquid CO_2 method) and different spectroscopic techniques were utilized to confirm the formation of its inclusion complex. Further, the double emulsion solvent evaporation method was used to load the MER-γ-CD inclusion complex into PLGA NPs to form MER-γ-CD NPs, showing that drug loading and entrapment efficiency was 3.6 and 42.1% *w/w*, respectively. In vitro release study showed that 27.4% of total drug (MER) were released from MER-γ-CD NPs in 8 h. This work also demonstrates the significant potential of dye loaded particles for intracellular uptake into intestinal cancer cells. However, this study showed that γ-CD or PLGA NPs were not able to improve the permeability of the drug or to reduce the rate of drug efflux in the Caco-2 cell monolayer model. Finally, it was shown that the encapsulation of MER with γ-CD and PLGA NPs retained MER's antibacterial activities against two bacterial strains such as *S. aureus* and *P. aeruginosa*. Overall, our proof of concept study paves the way to further investigate some other nano-carriers that may not only help to protect MER from gastric pH but also improve the drug permeation with reduced drug efflux.

CRediT authorship contribution statement

Aun Raza: Conceptualization, Formal analysis, Investigation, Methodology, Visualization, Writing - original draft, Writing - review & editing. **Jared A. Miles:** Methodology, Visualization, Writing - review & editing. **Fekade Bruck Sime:** Supervision, Writing - review & editing. **Benjamin P. Ross:** Methodology, Writing - review & editing. **Jason A. Roberts:** Supervision, Writing - review & editing. **Amirali Popat:** Conceptualization, Supervision, Writing - review & editing. **Tushar Kumeria:** Conceptualization, Formal analysis, Investigation, Methodology, Supervision, Visualization, Writing - original draft, Writing - review & editing. **James R. Falconer:** Conceptualization, Formal analysis, Investigation, Supervision, Writing - review & editing.

Declaration of Competing Interest

The authors declare that they have no known competing financial interests or personal relationships that could have appeared to influence the work reported in this paper.

Acknowledgments

Aun Raza is a recipient of the Australian Government Research Training Program Scholarship from The University of Queensland, Brisbane, Australia. The authors also thank Professor Andrew K. Whittaker of the Australian Institute for Bioengineering and Nanotechnology (AIBN), The University of Queensland, Brisbane, QLD 4072 Australia, for his support and access to specialized equipment, including the liquid CO_2 unit used in this research. T. K. acknowledges the support from the National Medical and Health Research Council of Australia for Early Career Fellowship (GNT1143296), Australian Research Council for Discovery Project (DP200102723), and the University of New South Wales for support and Scientia Grant. A.P. acknoldeges the support from National Health and Medical Research Council of Australia for Career

Development (GNT1146627), Early Career Fellowship (GNT1146627) and project grant. All the authors also acknowledge support from the Centre of Microscopy and Microanalysis and the School of Pharmacy's strategic research funds.

Appendix A. Supplementary material

Supplementary data to this article can be found online at https://doi.org/10.1016/j.ijpharm.2021.120280.

References

2010 2010. European Committee on Antimicrobial Susceptibility Testing.

2019 2019. EUCAST reading guide for broth microdilution.

2020 2020. European Committee on AntimicrobialSusceptibility Testing.

Artursson, P., Palm, K., Luthman, K., 2001. Caco-2 monolayers in experimental and theoretical predictions of drug transport. Adv. Drug Deliv. Rev. 46, 27–43.

AstraZeneca, Environmental Risk Assessment Data: Meropenem.

Avgoustakis, K., 2004. Pegylated poly (lactide) and poly (lactide-co-glycolide) nanoparticles: preparation, properties and possible applications in drug delivery. Curr. Drug Deliv. 1, 321–333.

Azad, M.A., Finnin, B.A., Poudyal, A., Davis, K., Li, J., Hill, P.A., Nation, R.L., Velkov, T., Li, J., 2013. Polymyxin B induces apoptosis in kidney proximal tubular cells. Antimicrobial Agents Chemotherapy 57, 4329–4335.

Baldwin, C.M., Lyseng-Williamson, K.A., Keam, J.S., 2008. Meropenem: A Review of its Use in the Treatment of Serious Bacterial Infections. Adis Drug Evaluation 68, 803–838.

Basu, T., Pal, B., Singh, S., 2016. Synthesis and characterization of ramipril embedded nanospheres of biodegradable poly-d, l-lactide-co-glycolide and their kinetic release study. Adv. Sci., Eng. Med. 8, 444–449.

Bergeon, J.A., Ziora, Z.M., Abdelrahim, A.S., Pernevi, N.U., Moss, A.R., Toth, I., 2010. In vitro and in vivo evaluation of positively charged liposaccharide derivatives as oral absorption enhancers for the delivery of anionic drugs. J. Pharm. Sci. 99, 2333–2342.

Blanco, M., Alonso, M., 1997. Development and characterization of protein-loaded poly (lactide-co-glycolide) nanospheres. Europ. J. Pharm. Biopharm. 43, 284–294.

Butkus, E., Martins, J.C., Berg, U., 1996. 1 H NMR spectroscopic study of the interaction between cyclodextrins and bicyclo [3.3. 1] nonanes. J. Inclusion Phenomena Mol. Recognition Chem. 26, 209-218.

Carrier, R.L., Miller, L.A., Ahmed, I., 2007. The utility of cyclodextrins for enhancing oral bioavailability. J. Control. Release 123, 78–99.

Cielecka-Piontek, J., Paczkowska, M., Lewandowska, K., Barszcz, B., Zalewski, P., Garbacki, P., 2013. Solid-state stability study of meropenem–solutions based on spectrophotometric analysis. Chem. Cent. J. 7, 98.

Craig, W.A., 1997. The pharmacology of meropenem, a new carbapenem antibiotic. Clin. Infect. Dis. 24, S266–S275.

Crist, G.B., 2009. Trends in Small-Volume Dissolution Apparatus for Low-Dose Compounds. Dissolution Technol. 16, 19–22.

Fawaz, S., Barton, S., Whitney, L., Swinden, J., Nabhani-Gebara, S., 2019. Stability of meropenem after reconstitution for administration by prolonged infusion. Hospital Pharm. 54, 190–196.

Ghaferi, M., Amari, S., Mohrir, B.V., Raza, A., Shahmabadi, H.E., Alavi, S.E., 2020a. Preparation, Characterization, and Evaluation of Cisplatin-Loaded Polybutylcyanoacrylate Nanoparticles with Improved In Vitro and In Vivo Anticancer Activities. Pharmaceuticals 13, 44.

Ghaferi, M., Koohi Moftakhari Esfahani, M., Raza, A., Al Harthi, S., Ebrahimi Shahmabadi, H., Alavi, S.E., 2020b. Mesoporous silica nanoparticles: synthesis methods and their therapeutic use-recent advances. J. Drug Targeting, 1-67.

Govender, T., Stolnik, S., Garnett, M.C., Illum, L., Davis, S.S., 1999. PLGA nanoparticles prepared by nanoprecipitation: drug loading and release studies of a water soluble drug. J. Control. Release 57, 171–185.

Guo, B., Xu, D., Liu, X., Liao, C., Li, S., Huang, Z., Li, X., Yi, J., 2017. Characterization and cytotoxicity of PLGA nanoparticles loaded with formononetin cyclodextrin complex. J. Drug Delivery Sci. Technol. 41, 375–383.

Huang, Y., Quan, P., Wang, Y., Zhang, D., Zhang, M., Li, R., Jiang, N., 2017. Host-guest interaction of β-cyclodextrin with isomeric ursolic acid and oleanolic acid: physicochemical characterization and molecular modeling study. J. Biomed. Res. 31, 395.

Job, P., 1928. Job's method of continuous variation. Ann. chim 9.

Joint, F., Additives, W.E.C.o.F., Organization, W.H., 2005. Evaluation of certain food additives: sixty-third report of the Joint FAO. World Health Organization.

Kankala, R.K., Zhang, Y.S., Wang, S.B., Lee, C.H., Chen, A.Z., 2017. Supercritical fluid technology: An emphasis on drug delivery and related biomedical applications. Adv. Healthcare Mater. 6, 1700433.

Kashi, T.S.J., Eskandarion, S., Esfandyari-Manesh, M., Marashi, S.M.A., Samadi, N., Fatemi, S.M., Atyabi, F., Eshraghi, S., Dinarvand, R., 2012. Improved drug loading and antibacterial activity of minocycline-loaded PLGA nanoparticles prepared by solid/oil/water ion pairing method. Int. J. Nanomed. 7, 221.

Kigen, G., Edwards, G., 2017. Drug-transporter mediated interactions between anthelminthic and antiretroviral drugs across the Caco-2 cell monolayers. BMC Pharmacol. Toxicol. 18, 20.

Lamson, N.G., Berger, A., Fein, K.C., Whitehead, K.A., 2020. Anionic nanoparticles enable the oral delivery of proteins by enhancing intestinal permeability. Nat. Biomed. Eng. 4, 84–96.

Lee, S.-Y., Jung, I.-I., Kim, J.-K., Lim, G.-B., Ryu, J.-H., 2008. Preparation of itraconazole/HP-β-CD inclusion complexes using supercritical aerosol solvent extraction system and their dissolution characteristics. J. Supercritical Fluids 44, 400–408.

Lim, Y.H., Tiemann, K.M., Hunstad, D.A., Elsabahy, M., Wooley, K.L., 2016. Polymeric nanoparticles in development for treatment of pulmonary infectious diseases. Wiley Interdisciplinary Rev.: Nanomed. Nanobiotechnol. 8, 842-871.

Lina, B., Bär, A.J.R.T., Pharmacology, 2004. Subchronic oral toxicity studies with α-cyclodextrin in rats. 39, 14-26.

Mendez, A.S., Dalomo, J., Steppe, M., Schapoval, E.E., 2006. Stability and degradation kinetics of meropenem in powder for injection and reconstituted sample. J. Pharm. Biomed. Analy. 41, 1363-1366.

Mendez, A.S., Steppe, M., Schapoval, E.E., 2003. Validation of HPLC and UV spectrophotometric methods for the determination of meropenem in pharmaceutical dosage form. J. Pharm. Biomed. Analy. 33, 947-954.

Nicolau, D.P., 2008. Pharmacokinetic and Pharmacodynamic Properties of Meropenem. Clin. Infect. Dis. 47, S32–S40.

Paczkowska, M., Mizera, M., Szymanowska-Powałowska, D., Lewandowska, K., Błaszczak, W., Gościańska, J., Pietrzak, R., Cielecka-Piontek, J., 2016. β-Cyclodextrin complexation as an effective drug delivery system for meropenem. Eur. J. Pharm. Biopharm. 99, 24–34.

Pasquali, I., Bettini, R., 2008. Are pharmaceutics really going supercritical? Int. J. Pharm. 364, 176–187.

Pelgrift, R.Y., Friedman, A.J., 2013. Nanotechnology as a therapeutic tool to combat microbial resistance. Adv. Drug Deliv. Rev. 65, 1803-1815.

Rasheed, A., 2008. Cyclodextrins as drug carrier molecule: a review. Sci. Pharm. 76, 567–598.

Raza, A., Bano, S., Xu, X., Zhang, R.X., Khalid, H., Iqbal, F.M., Xia, C., Tang, J., Ouyang, Z., 2017a. Rutin–nickel complex: synthesis, characterization, antioxidant, DNA binding, and DNA cleavage activities. Biol. Trace Elem. Res. 178, 160–169.

Raza, A., Ngieng, S.C., Sime, F.B., Cabot, P.J., Roberts, J.A., Popat, A., Kumeria, T., Falconer, J.R., 2020. Oral meropenem for superbugs: challenges and opportunities. Drug Discovery Today.

Raza, A., Sun, H., Bano, S., Zhao, Y., Xu, X., Tang, J., 2017b. Preparation, characterization, and in vitro anti-inflammatory evaluation of novel water soluble kamebakaurin/hydroxypropyl-β-cyclodextrin inclusion complex. J. Mol. Struct. 1130, 319-326.

Raza Aun, F.B.S., Peter J. Cabot, Jason A. Roberts, James R. Falconer, Tushar Kumeria,, Popat, A.A., 2020. Liquid CO2 Formulated Mesoporous Silica Nanoparticles for pH Responsive Oral Delivery of Meropenem. ACS Biomater. Sci. Eng.

Saito, T., Sawazaki, R., Ujiie, K., Oda, M., Saitoh, H., 2012. Possible factors involved in oral inactivity of meropenem, a carbapenem antibiotic. Pharmacol. Pharm. 3, 6.

Sarti, F., Perera, G., Hintzen, F., Kotti, K., Karageorgiou, V., Kammona, O., Kiparissides, C., Bernkop-Schnürch, A., 2011. In vivo evidence of oral vaccination with PLGA nanoparticles containing the immunostimulant monophosphoryl lipid A. Biomater. Sci. 32, 4052–4057.

Sherman, G., Shenoy, S., Weiss, R., Erkey, C., 2000. A static method coupled with gravimetric analysis for the determination of solubilities of solids in supercritical carbon dioxide. Ind. Eng. Chem. Res. 39, 846-848.

Shirasaka, Y., Sakane, T., Yamashita, S., 2008. Effect of P-glycoprotein expression levels on the concentration-dependent permeability of drugs to the cell membrane. J. Pharm. Sci. 97, 553–565.

Singh, R., Bharti, N., Madan, J., Hiremath, S., 2010. Characterization of cyclodextrin inclusion complexes—a review. Pharm. Sci. Technol 2, 171–183.

Talaczyńska, A., Lewandowska, K., Garbacki, P., Zalewski, P., Skibiński, R., Miklaszewski, A., Mizera, M., Cielecka-Piontek, J., 2016. Solid-state stability studies of crystal form of tebipenem. Drug Dev. Ind. Pharm. 42, 238–244.

Tang, P., Li, S., Wang, L., Yang, H., Yan, J., Li, H., 2015. Inclusion complexes of chlorzoxazone with β-and hydroxypropyl-β-cyclodextrin: characterization, dissolution, and cytotoxicity. Carbohydr. Polym. 131, 297–305.

Vaidya, B., Parvathaneni, V., Kulkarni, N.S., Shukla, S.K., Damon, J.K., Sarode, A., Kanabar, D., Garcia, J.V., Mitragotri, S., Muth, A., 2019. Cyclodextrin modified erlotinib loaded PLGA nanoparticles for improved therapeutic efficacy against non-small cell lung cancer. Int. J. Biol. Macromol. 122, 338–347.

Weinstein, M.P., Lewis, J.S., 2020. The Clinical and Laboratory Standards Institute Subcommittee on Antimicrobial Susceptibility Testing: Background, Organization, Functions, and Processes. J. Clin. Microbiol. 58, 1–7.

Wong, J., Kipp, J.E., Miller, R.L., Nair, L.M., Ray, G.J., 2014. Mechanism of 2-hydroxypropyl-beta-cyclodextrin in the stabilization of frozen formulations. Europ. J. Pharm. Sci.: Off. J. Europ. Federat. Pharm. Sci. 62, 281-292.

Xiao, C.-F., Li, K., Huang, R., He, G.-J., Zhang, J.-Q., Zhu, L., Yang, Q.-Y., Jiang, K.-M., Jin, Y., Lin, J., 2014. Investigation of inclusion complex of epothilone A with cyclodextrins. Carbohydr. Polym. 102, 297–305.

Yáñez, C., Cañete-Rosales, P., Castillo, J.P., Catalán, N., Undabeytia, T., Morillo, E., 2012. Cyclodextrin inclusion complex to improve physicochemical properties of herbicide bentazon: exploring better formulations. PLoS ONE 7, e41072.

Yang, L.-J., Chen, W., Ma, S.-X., Gao, Y.-T., Huang, R., Yan, S.-J., Lin, J., 2011. Host–guest system of taxifolin and native cyclodextrin or its derivative: Preparation, characterization, inclusion mode, and solubilization. Carbohydr. Polym. 85, 629–637.

Zhang, L., Pornpattananangkul, D., Hu, C.-M., Huang, C.-M., 2010. Development of nanoparticles for antimicrobial drug delivery. Curr. Med. Chem. 17, 585–594.